Sensors & Diagnostics

Accepted Manuscript

This article can be cited before page numbers have been issued, to do this please use: H. Hu, T. Wang, B. Zhang, K. Jin, Z. Wang, Q. Huang, H. Ma, J. Li, Z. Chen and S. Hu, *Sens. Diagn.*, 2025, DOI: 10.1039/D6SD00032K.

View Article Online
DOI: 10.1039/D6SD00032K

ARTICLE

Single-Nucleotide Polymorphisms Detection Base on Active-Matrix Digital Microfluidics Pyrosequencing Lab-on-a-chip Platform

Received 00th January 20xx,
Accepted 00th January 20xx

DOI: 10.1039/x0xx00000x

Huiting Hu,†[a] Tong Wang,†[b] Bingbing Zhang,[a] Kai Jin,[c] Zihan Wang,[d] Qi Huang,[c] Hanbin Ma,[b] Jinhua Li,[a*] Zhiyao Chen,[d*] Siyi Hu[c*]

Single-nucleotide polymorphisms (SNPs), as the most prevalent form of single-base variations within the genome, play a critical role in modulating protein function, regulating gene expression, and determining individual disease susceptibility, thereby serving as key biomarkers in personalised medicine. Currently, the mainstream method for detecting SNPs in known short sequences is pyrosequencing, yet this approach faces limitations such as complex operational procedures and limited automation. Digital microfluidics (DMF) provides an ideal platform for accomplishing complex biochemical processes through electrically programmable manipulation of discrete droplets, thereby simplifying operational procedures. In this study, we report the design of a pyrosequencing system based on an active-matrix digital microfluidic (AM-DMF) chip. This work represents the first demonstration of combining AM-DMF with pyrosequencing for on-chip SNP genotyping, enabling direct and automated genetic analysis within a sinlge microfluidics platform. This fills a gap in the DMF platform for pharmacogenomics SNPs detection. Compared with conventional passive-matrix digital microfluidics (PM-DMF), the AM-DMF offers greater scalability and higher electrode utilisation, making it well suited for larger-scale integration and high-throughput applications. This study utilized DNA samples from 12 patients to achieve rapid assessment of clopidogrel metabolism through genotyping of the *CYP2C19*2* and **3* loci. Experimental results demonstrate that the system completes on-chip testing of a single sample analysis in under 30 minutes, with results reaching 100% accuracy in total agreement with the commercial pyrosequencer (PyroMark Q24). Furthermore, reagent consumption was reduced by approximately 50%, significantly lowering per-sample cost. These results indicate that the proposed AM-DMF-based pyrosequencing platform enables rapid, accurate, and cost-effective SNPs detection, and holds substantial potential for clinical applications in precision and personalised medicine.

1 Introduction

DNA sequencing enables the direct acquisition of primary genetic information by resolving the nucleotide sequence of DNA molecules, thereby determining their structure and function. In the medical field, DNA sequencing is essential for research on mutation localization, identification, and comparison, aiding in the diagnosis, prevention, and treatment of diseases[1]. The rapid advancement of DNA sequencing technology has greatly propelled the development of biomedicine, leading to significant progress in genomics, genetics, molecular diagnostics, and other related fields.

Pyrosequencing is a DNA sequencing technique based on enzyme-cascade reactions. Compared with traditional sequencing methods, it offers precise quantification, rapid analysis, and cost-effectiveness[2]. Pyrosequencing technology enables direct determination of the sequence of target nucleic acid fragments, earning it recognition as the gold standard in molecular diagnostics. With ongoing technological refinement and advancement, pyrophosphate sequencing will assume an increasingly pivotal role across genomics, genetics, and transcriptomics. This technique holds promise to provide robust support for developments in personalised medicine and precision medicine.

Single nucleotide polymorphisms (SNPs) denote a form of DNA sequence polymorphism arising from variation in a single nucleotide within genomic DNA sequences. The human genome contains tens of millions of SNPs, representing the most prevalent form of variation within the genome. These polymorphisms are implicated in disease onset, responses to pathogens and medications, and exert significant influence on individual drug metabolism capabilities and susceptibility to disease. Pyrosequencing demonstrates distinct advantages in SNPs detection due to its high throughput, sensitivity, and accuracy[3]. By continuously monitoring pyrophosphate release during sequencing, this technique precisely identifies single-base differences, circumventing the complex steps of electrophoresis separation or fluorescent labelling in conventional sequencing. It is particularly suited for rapid screening of low-frequency mutations in

[a] Nanophotonics and Biophotonics Key Laboratory of Jilin Province, Changchun University of Science and Technology, Changchun, 130022, P.R.China.
[b] Department of Laboratory Medicine, Sichuan Provincial People's Hospital, School of Medicine, University of Electronic Science and Technology of China, Chengdu, Sichuan province, 610072, P.R.China.
[c] CAS Key Laboratory of Bio-medical Diagnostics, Suzhou Institute of Biomedical Engineering and Technology, Chinese Academy of Sciences, No. 88 Keling Road, Suzhou, Jiangsu province, 215163, P.R.China.
[d] Department of Pharmacy, The First Affiliated Hospital of Soochow University, Suzhou, 215006, P.R.China.
†These authors contributed equally to the work.
* Corresponding author: husiyi@sibet.ac.cn. lijh@cust.edu.cn.
Zhiyao_czy@163.com
Electronic Supplementary Information (ESI) available: [details of any supplementary information available should be included here]. See DOI: 10.1039/x0xx00000x

clinical samples[4, 5]. Specific genomic SNPs may influence responsiveness to drug therapies, establishing SNPs as a key predictive factor in pharmacogenomics[6].

Despite these advantages, conventional pyrosequencing systems remain constrained by bulky instrumentation, limited automation, and relatively high reagent consumption, which restrict their deployment in decentralised or resource-limited clinical settings. To address these challenges, digital Microfluidics (DMF) has emerged as a powerful technology for miniaturised biochemical analysis[7]. DMF, typically based on the electrowetting-on-dielectric (EWOD) principle, which enables precise manipulation of droplets in the microliter to nanoliter range through programmable electric fields. Operations such as dispensing, moving, mixing, separating, storing, reacting, or analysing droplets can be performed, and specific workflows can be automated by programming the electrode arrays[8, 9]. Active-Matrix Digital Microfluidics (AM-DMF) integrates a thin-film transistor (TFT) at each pixel, allowing independent control within large-scale arrays[10]. The advantage of the active matrix is that an array of N (rows) × M (columns) requires only N + M control lines [11, 12]. In the ideal Active-Matrix Electrowetting-on-Dielectric (AM-EWOD) system, each pixel independently drives a droplet, thereby achieving the best control accuracy, the highest array utilization efficiency, and the best stability[13].

Previous studies have demonstrated the feasibility of integrating pyrosequencing with digital microfluidics. In 2007, the Fair research group at Duke University in the United States constructed a digital microfluidic chip for pyrosequencing. The designed sequencing workflow enabled simultaneous reactions and detection, significantly reducing sequencing time[14]. In 2011, Welch et al. from Duke University designed a pyrosequencing system using a digital microfluidic chip, achieving successful sequence detection[15, 16]. In 2019, Yang's team from Xiamen University conducted single-channel sequencing experiments using a designed digital microfluidic pyrosequencing platform[17]. However, to date, digital microfluidics has not been applied to pharmacogenomic SNPs detection using an active-matrix architecture, and challenges related to high-throughput, scalability and clinical adaptability remain largely unexplored.

Compared to PM-DMF, the AM-DMF architecture provides significant advantages that are particularly beneficial for complex biochemical assays like pyrosequencing: Elimination of Crosstalk and Parasitic Actuation: In PM systems, electrodes are driven by row and column lines, which often leads to unintended "crosstalk" or parasitic actuation of neighboring droplets. Our AM-DMF platform uses an integrated TFT array to provide independent and precise control of each electrode, ensuring high-fidelity droplet manipulation during the rigorous multi-step nucleotide dispensing cycles of pyrosequencing.High-Resolution Multi-Reagent Integration: Pyrosequencing requires the precise coordination of multiple reagents (enzymes, substrates, and four dNTPs). The high-density AM array allows for the simultaneous storage and routing of these diverse reagents on a single chip, whereas PM systems are often limited by electrode routing constraints when handling more than 3-4 reagent types. Scalability for High-Throughput Sequencing: AM-DMF overcomes the "pin-count" bottleneck. While PM systems require an increasing number of connections as the array grows, AM-DMF can control thousands of pixels with a fixed number of gate/data lines. This provides a tangible pathway for scaling up from single-SNP detection to large-scale, multiplexed genomic analysis.

Advancements in Pyrosequencing: By leveraging AM-DMF, we have achieved a highly automated, programmable sequencing workflow that reduces human error and reagent consumption compared to conventional platforms. This work represents a key step toward a high-density "sequencing-on-a-chip" architecture.

Based on the above research basis and our research needs, We have integrated AM-DMF technology with pyrosequencing to establish a SNPs detection system, optimising the operational workflow. By integrating the entire pyrosequencing reaction process onto an AM-DMF chip, we have significantly simplified the procedure, ensured the stability and reliability of the sequencing process, and enhanced the level of sequencing automation. This facilitates streamlined sequencing, instrument miniaturization, and reduced costs. Leveraging the system's cost-effectiveness and customizability, its application can be extended to scenarios such as DNA methylation analysis[18], pathogen identification[19], and bacterial strain typing[20].

2 Experimental

2.1 Pyrosequencing principle

The pyrosequencing process can be represented by the following cascade reactions, as shown in equations (1)-(3). When a deoxynucleotide triphosphate (dNTP) is added and incorporated into the DNA template by DNA polymerase, pyrophosphate (PPi) is released. ATP sulfurylase catalyzes the reaction between pyrophosphate and adenosine 5'-phosphosulfate (APS) to produce adenosine triphosphate (ATP). The fluorescent enzyme catalyzes the reaction between ATP and luciferin to form oxyluciferin, thereby emitting visible light with a wavelength of approximately 560 nm. This light signal can be detected by a photomultiplier tube (PMT) or a charge-coupled device (CCD) and used to record the nucleotide sequence of the template DNA in real time[21, 22], characterized by peak patterns. The dNTPs and small amounts of ATP remaining in the reaction system are degraded by apyrase[16], as shown in equations (4) and (5).

$$(\mathbf{DNA})_{\mathbf{n}} + \mathbf{dNTP} \xrightarrow{\mathbf{DNA\ polymersae}} (\mathbf{DNA})_{\mathbf{n+1}} + \mathbf{PPi} \quad (1)$$

$$\mathbf{PPi} + \mathbf{APS} \xrightarrow{\mathbf{ATP\ sulphurylase}} \mathbf{ATP} + \mathbf{SO_4^{-2}} \quad (2)$$

$$\mathbf{ATP} + \mathbf{luciferin} + \mathbf{O_2} \xrightarrow{\mathbf{luciferase}} \mathbf{AMP} + \mathbf{PPi} + \mathbf{CO_2} + \mathbf{oxyluciferin} + \mathbf{hv} \quad (3)$$

$$\mathbf{dNTP} \xrightarrow{\mathbf{Apyrase}} \mathbf{dNDP} + \mathbf{dNMP} + \mathbf{phosphate} \quad (4)$$

$$\mathbf{ATP} \xrightarrow{\mathbf{Apyrase}} \mathbf{ADP} + \mathbf{AMP} + \mathbf{phosphate} \quad (5)$$

2.2 Reagents and materials

The PyroMark PCR Kit, PyroMark Gold Q96 Reagents, PyroMark Binding Buffer, PyroMark Denaturation Solution, PyroMark Wash Buffer and PyroMark Annealing Buffer were all purchased from

View Article Online
DOI: 10.1039/D5SD00078K

QIAGEN (Shanghai, China). The Qubit™ dsDNA Assay Kit was obtained from Thermo Fisher Scientific (USA). Streptavidin-coated magnetic beads (CMP1001SA) were sourced from Suzhou Weidu Biotechnology (China). PCR primers (forward and reverse), sequencing primers, and the standard sequence were all synthesized by Genewiz (Suzhou, China).

In the *CYP2C19* gene detection experiments, all samples were derived from blood samples from subjects in the Phase I Clinical Trial of the First Affiliated Hospital of Soochow University. All experiments were performed in accordance with the Guidelines the Declaration of Helsinki, and approved by the Institutional Ethics Committee of the First Affiliated Hospital of Soochow University (Project Name: CYP2C19 Genotype Assay Kit, Ethics Registration Number: 2021069).

2.3 Amplifications assay

The total reaction volume for PCR was 20 μL, comprising 3 μL of DNA template, 12.5 μL of reaction solution, 0.5 μL each of 10 μM forward and reverse primers, and 8.5 μL of enzyme-free water. The amplification protocol (95°C for 10 min; 45 cycles of 94°C for 30 s, 60°C for 30 s, 72°C for 30 s; and final extension at 72°C for 10 min) was executed. The specific sequence is shown in Table S1.

In the *CYP2C19* gene detection experiment, the total PCR reaction volume was 40 μL, which included 2 μL DNA template, 13.5 μL reaction solution, 0.5 μL DNA polymerase, and 24 μL enzyme-free water. The amplification procedure (95°C for 10 minutes; 95°C for 30 seconds, 60°C for 30 seconds, 72°C for 30 seconds, and 72°C for 7 minutes) was carried out for 35 cycles. The specific sequence is shown in Table S2.

2.4 Sample Preparation

As the forward PCR primer was biotinylated, one strand of the PCR product incorporated biotin, enabling specific binding to streptavidin-coated magnetic beads. The reaction system consisted of 10 μL of PCR product, 13 μL of magnetic beads (10 mg/mL), 20 μL of enzyme-free water, and 9 μL of binding buffer. The mixture was agitated at 1400 rpm for 5 to 10 minutes at room temperature, after which the supernatant was removed. The mixture was washed with enzyme-free water. Subsequently, the DNA double-strands were denatured into single-strand using Denaturation Solution. The biotinylated single-strand were collected using a magnet, the supernatant was removed, and the strands were washed with Wash Buffer. Then, 10 μL of sequencing primer solution (diluted to 0.375 μM with Annealing Buffer) was added. The mixture was heated at 80°C for five minutes and cooled to room temperature to allow the sequencing primer to anneal to the template strand. This process takes place entirely off-chip.

2.5 Fabrication of AM-DMF Chips

The AM-DMF chip provides a platform for sequencing reactions. The structural of the chip is shown in Figure 1(a). It mainly consists of a top plate, a bottom plate, a ground electrode, a dielectric layer, a hydrophobic layer, and actuation electrode arrays. The physical chip is shown in Figure 1(b). The top plate of the DMF chip is a glass substrate coated with indium tin oxide (ITO). The bottom plate of the chip contains a series of DMF actuation electrodes. The surface of the electrodes is coated with a 300 nm thick silicon nitride film (SiNx) as the dielectric layer. Ultrasonic cleaning of the top plate and the bottom plate, followed by drying on a hot plate (180°C for 5 minutes). A layer of 2% Teflon with a thickness of 300 nm is spin-coated on the bottom plate and the top plate respectively as a hydrophobic layer. The chips were baked on a hot plate (40℃ for 10 minutes; 180℃ for 20 minutes) to cure the hydrophobic layer. Apply conductive silver paste to the base plate to form an electrical circuit when the base plate and top cover make contact. The top plate and the bottom plate are separated by 400 μm spacer. Finally, heat-press the FPC to the connection point of the film pins. The volume of each driving electrode is 25 nL. For more detailed information, please refer to Figure S1.

2.6 Establishment of the SNPs Detection System

The pyrosequencing system based on DMF is shown in Figure 1(c). The system consists of an AM-DMF control module, optical fibre assembly, focusing optics, a single-photon counting photomultiplier tube (PMT, CH299, Hamamatsu, Japan), and a photon counting unit (CH297, Hamamatsu, Japan). The digital microfluidics module includes control software, a driving circuit, the AM-DMF chip, a light-shielding enclosure, and a magnetic module. The chip was electrically interfaced with the control board via 128 flexible printed circuit (FPC) signal lines. Droplet actuation was achieved by applying a 60 V driving voltage between the top and bottom plates. The control software is primarily used to apply voltage to the AM-DMF chip within specific areas and to record its position; this allows the droplet's reaction path to be designed in advance within the software and saved as a file. During the experiment, one simply needs to open the file and run the process along the pre-set path to achieve automatic droplet control. Chemiluminescent signals generated during pyrosequencing were collected by the PMT and transmitted to a computer for real-time data acquisition. All measurements were conducted in a dark environment with additional light shielding to minimise background interference.

2.7 Signal Acquisition and Processing

The faint photons generated by the pyrosequencing reaction are collimated and focused through an optical fibre lens, then transmitted via fibre optic cable to the photocathode of the photomultiplier tube (PMT). Through the photoelectric effect, photoelectrons enter the multiplication system where they are amplified into measurable electrical pulses. This signal undergoes discrimination and shaping to form a standard pulse (TTL) output, which is then counted by the photon counter. The count is transmitted to a computer to yield the luminescence intensity. For the raw photon count detected, background noise signals are first subtracted, and the measured peak height is then recorded as the final data. By analysing the collected light intensity, the number of nucleotide homopolymers bound to the DNA strand can be determined. Since the types of added nucleotides are known, the base sequence can be deduced.

View Article Online
DOI: 10.1039/D6SD00032K

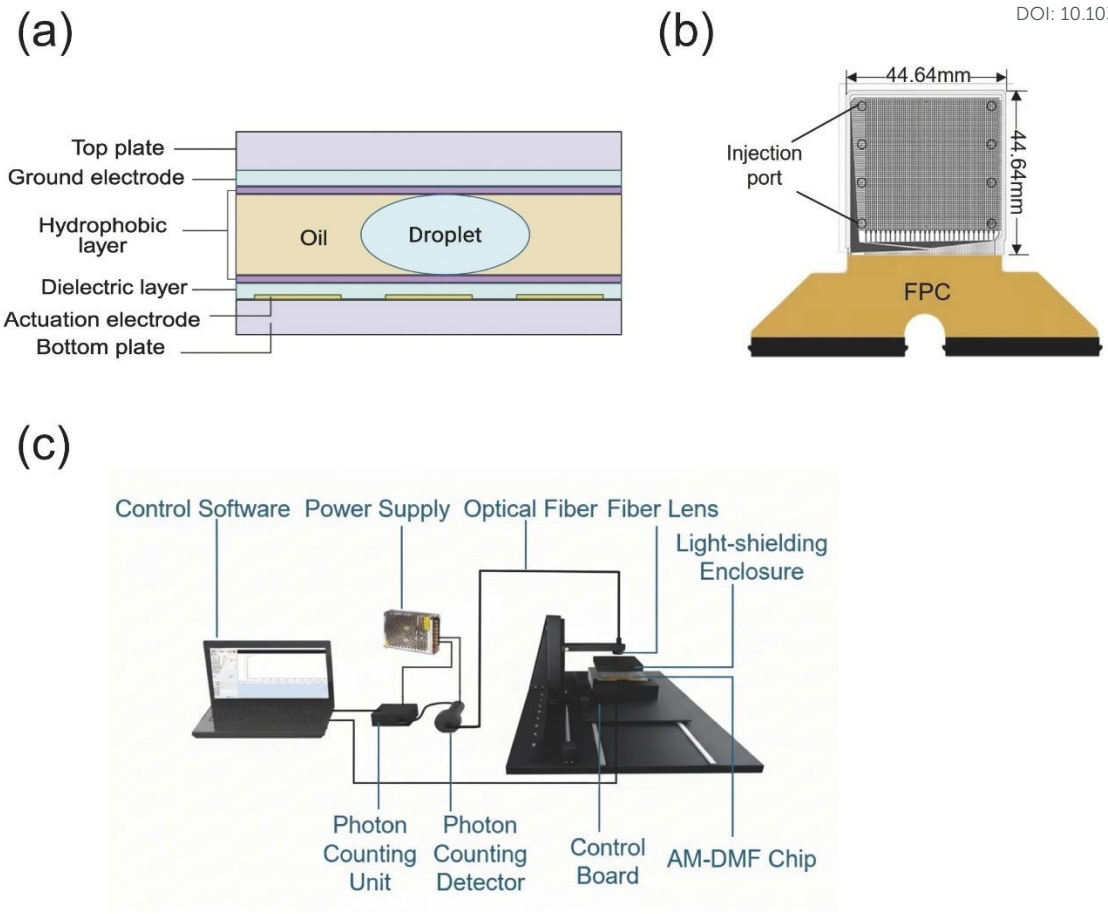

Fig.1 Pyrosequencing system based on AM-DMF. (a) Schematic diagram of the cross-sectional structure of the chip. (b) Schematic diagram of an AM-DMF chip. (c) Image of the pyrosequencing system based on AM-DMF.

2.8 Pyrosequencing system workflow

The complete pyrosequencing workflow is illustrated in Figure 2. Sample pre-processing was first performed off-chip, as shown in Figure 2(a). Silicone oil is injected into the chip, followed by the addition of the processed DNA fragments, enzyme mixture (DNA polymerase, ATP sulfurylase, luciferase, diphosphatase, single-stranded DNA binding protein), a substrate mixture (5'-phosphoadenosine 5'-sulfate, luciferin), and the four nucleotides (dATP, dTTP, dCTP, dGTP), as depicted in Figure 2(c). The pyrosequencing principle is illustrated in Figure 2(b), where the chip is partitioned into reagent reservoir zones, waste zones, reaction zones, and detection zones as depicted in Figure 2(d). The specific reaction workflow is shown in Figure 2(e): (1) 10 µL of sample was added and fixed with a magnet; the supernatant was then transferred to the waste liquid area. (2) 3.5 µL of enzyme and substrate were added to resuspend the sample, which was mixed thoroughly by movement across multiple electrodes. (3) One nucleotide was added and mixed with the sample in the detection area by manipulating different-sized droplets; light signals were collected for approximately one minute using the PMT. 240 data points were counted at 250 ms intervals. (4) Step (3) was repeated four times. (5) The supernatant was removed, and steps (2-4) were repeated in a specific sequence.

Nucleotides were dispensed in a predetermined sequence to ensure that the incorporation reaction proceeded to completion. At intervals of every four reaction cycles, the supernatant was extracted, and the enzyme and substrate mixtures were replenished; this step was critical to mitigate the dilution effects resulting from the cumulative increase in total reaction volume and to prevent the

View Article Online
DOI: 10.1039/D6SD00032K

ARTICLE

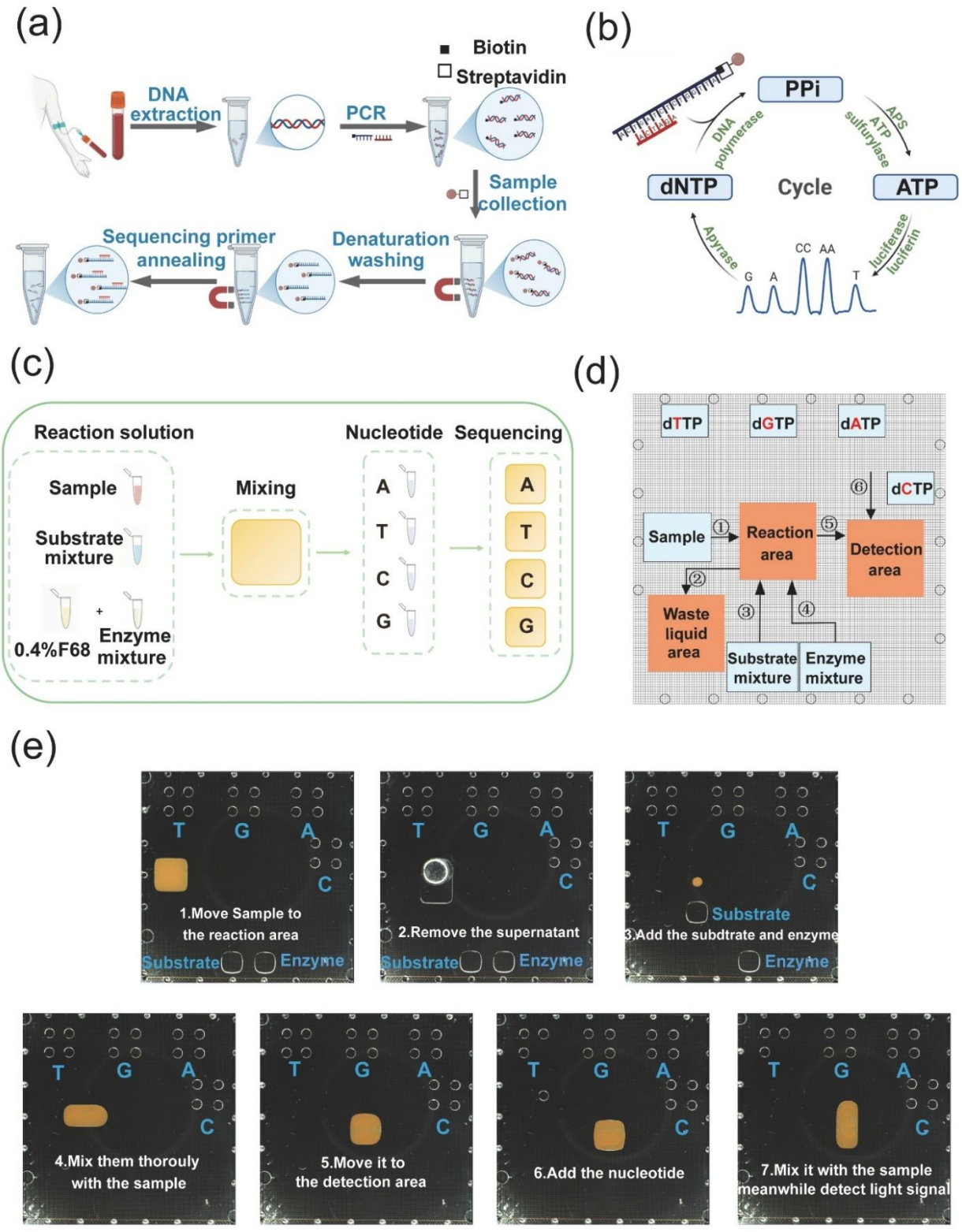

Fig.2 Pyrosequencing workflow. (a) Sample Pre-processing Procedure. (b) The principle of pyrosequencing. (c) Schematic diagram of on-chip sequencing. (d) Reagent partitioning diagram on the chip. (e) On-chip practical demonstration diagram.

View Article Online
DOI: 10.1039/D6SD00032K

ARTICLE

attenuation of the optical signal. Furthermore, given that the enzyme mixture incorporates a bisphosphatase capable of effectively degrading residual nucleotides and ATP, the protocol did not require a dedicated washing step to eliminate the luminescent signal background. Upon completion of the reaction, the nucleotide sequence was quantitatively determined by analysing the intensity of the detected chemiluminescent light signals.

3 Results and Discussion

3.1 Performance Characterisation of the AM-DMF Chip

Droplet operations including transport, mixing, and splitting were achieved through programmable voltage actuation of the electrode array. In DMF system, minute fluctuations in droplet volume can significantly alter the composition of the reaction system, thereby critically influencing final outcomes. It is therefore necessary to characterise the uniformity of droplet generation and the stability of droplet motion on the AM-DMF chip to ensure reliable system performance.

As shown in Figure 3(a), a droplet tearing experiment was conducted to assess droplet uniformity. The tearing process involves positioning the droplet on the central drive electrode unit, where it contacts the drive electrode units on either side. When voltage is applied to the lateral electrode units while the central unit remains deactivated, the contact angles at the lateral interfaces decrease, causing the droplet to expand laterally. Ultimately, it splits into two smaller microdroplets. ImageJ software was employed to analyse droplet images, yielding the droplet base area as depicted in Figure 3(b). Further calculation of the coefficient of variation (CV) for the base area revealed a value of 2.26%, providing visual confirmation of the uniformity in droplet generation. In the single-droplet motion stability test, droplets continuously traveled along a circular path formed by eight electrodes. Three experimental groups were simultaneously set up in three different areas on the chip (Area A, Area B, and Area C), as shown in Figure S2 and 3(c). The droplet exhibited stable and repeatable motion without noticeable deformation or pinning, demonstrating the robust droplet control capability of the AM-DMF.

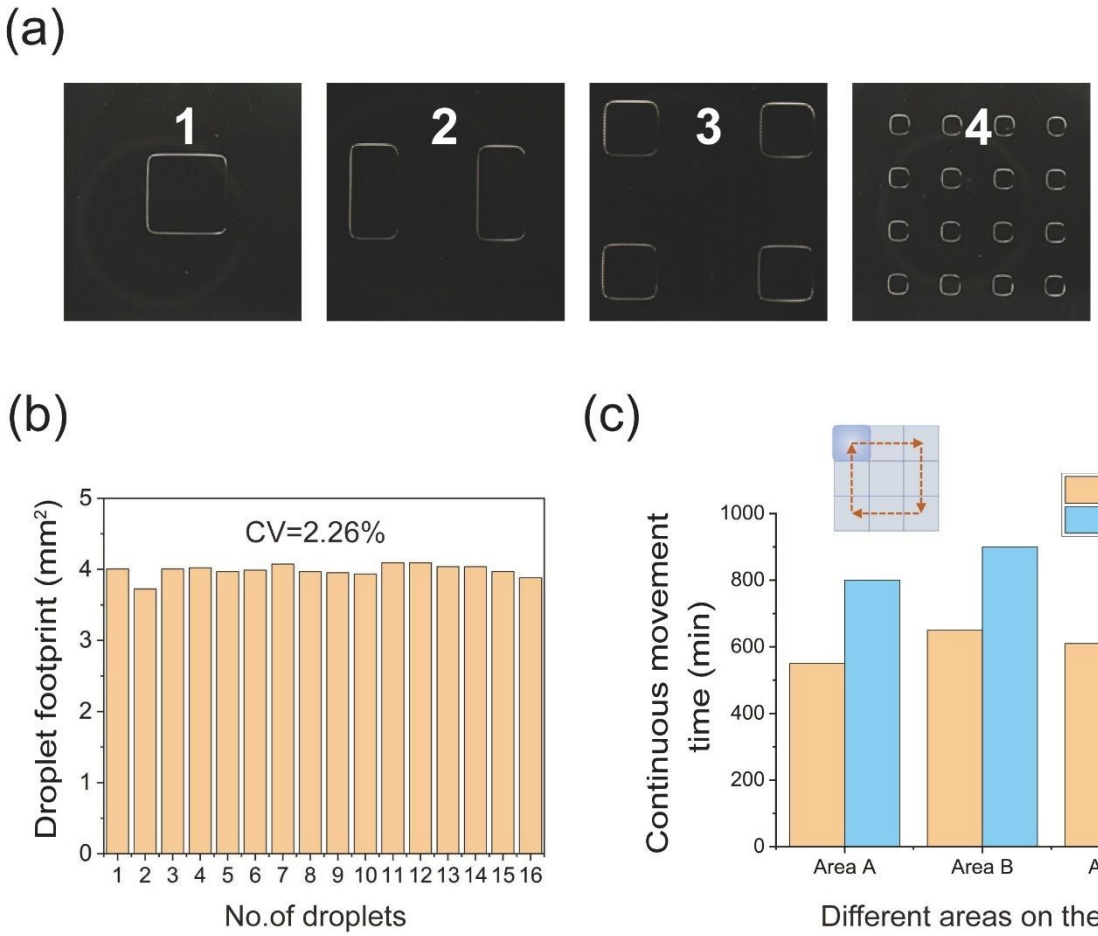

Fig.3 AM-DMF Chip Performance Characterisation. (a) Schematic of droplet tearing process. (b) Droplet Tear Uniformity. (c) The stability test of single droplet movement across different area (area A, area B, area C) on the same chip.

View Article Online
DOI: 10.1039/D6SD00032K

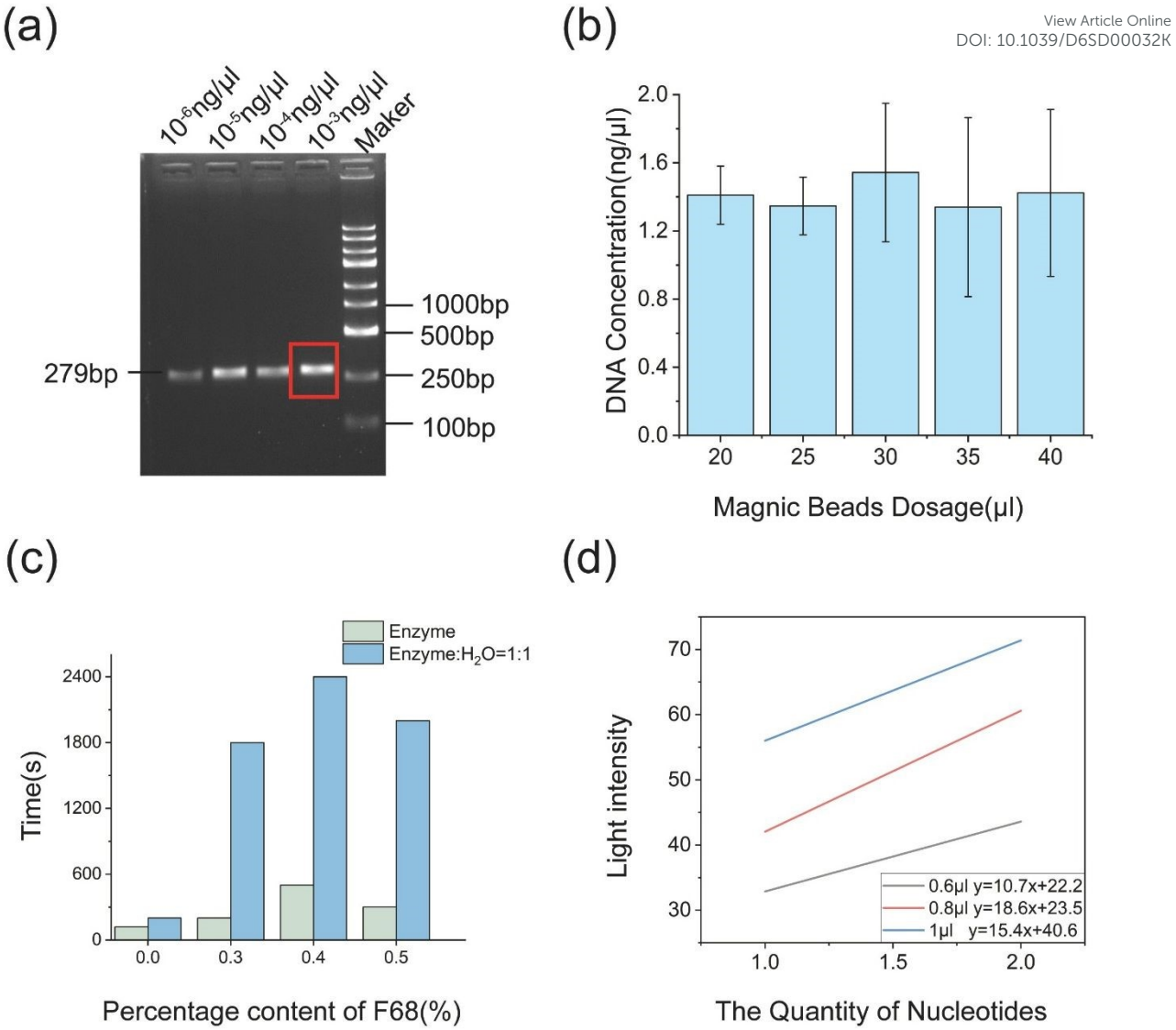

Fig.4 Reaction System Optimization and Validation. (a) Agarose gel electrophoresis results. (b) Gradient diagram of magnetic bead input quantity experiment results. (c) Stability Assessment of Reagent Mobility on the Chip. (d) The linear relationship between the number of nucleotides and signal intensity.

3.2 Optimization of experimental procedures

To validate the quality of PCR products, four template concentrations were prepared in a gradient of 10^{-3} to 10^{-6} ng/μL. These four samples were subjected to agarose gel electrophoresis. As shown in Figure 4(a), the bands were singular and distinct. All four samples successfully yielded the target DNA fragment of approximately 279 bp, indicating good DNA sample integrity with no apparent degradation. It is evident that the band obtained at the 10^{-3} ng/μL concentration was the brightest. Consequently, this concentration was selected for subsequent experiments.

The specific binding between streptavidin and biotin can efficiently capture and fix the double-stranded DNA molecules with biotin labels at the 5' end. This step replaces the purification of PCR products. The quantity of magnetic beads directly influences the effective DNA recovery yield, which in turn affects the intensity of the subsequent chemiluminescent signal[23]. Insufficient input will lead to insufficient binding, resulting in sample loss; while excessive input can ensure complete binding, but it may increase non-specific adsorption or complicate the subsequent elution steps. The amount of recovered DNA templates directly determines the number of active molecules of enzyme and substrate in the subsequent pyrosequencing reaction, making it a key factor in final chemiluminescence signal intensity. A gradient experiment was designed. After the binding and magnetic separation of magnetic beads and biotinylated DNA products were completed, the supernatant after the reaction was taken out, and the DNA content was detected using Qubit to determine the lost DNA. As demonstrated in Figure 4(b), experimental validation indicated that adding 25 μL of magnetic beads resulted in the least DNA loss. Consequently, 25 μL was selected as the subsequent addition volume.

Prior to formally injecting reagents into the chip for experimentation, their mobility within the chip environment must be assessed. All reagents except the enzyme mixture exhibited favorable flow characteristics. The enzyme mixture, containing high concentrations of protein macromolecules, these molecules readily adsorb onto the polymeric surface of the chip, leading to a significant reduction in overall migration efficiency[24, 25]. To improve the migration efficiency of the enzyme mixture, two approaches were employed: firstly, appropriate dilution to reduce protein concentration; secondly, the introduction of the non-ionic surfactant Pluronic F68, which exhibits excellent biocompatibility[26], to modify the liquid-solid interface properties and reduce non-specific adsorption. The droplet was moved back and forth between multiple electrodes to record the migration time. Droplet motion failure occurs when the droplet's movement cannot be controlled by applying voltage. Experimental verification, as shown in Figure 4(c), determined the optimal migration conditions to be diluting the enzyme mixture with ultrapure water at a 1:1 ratio while simultaneously adding 0.4% Pluronic F68.

The volume of nucleotide addition was optimized through the design of gradient experiments. It was determined that dNTPs could not be added in insufficient quantities, as this resulted in incomplete reactions; specifically, complementary bases on the template strand were not adequately incorporated, yielding weak sequencing signals that occasionally fell below the instrument's detection limit, thereby causing sequencing failure. Furthermore, low dNTP concentrations were found to prolong reaction times, as the enzyme required a longer duration to locate sufficient substrate, consequently reducing the overall efficiency of the sequencing process. Conversely, excessive dNTP addition was also deemed undesirable. High dNTP concentrations potentially induced non-specific binding, where non-complementary dNTPs were erroneously incorporated despite the lack of template complementarity, thereby introducing base errors and compromising sequencing accuracy. Simultaneously, this accelerated the dilution of the reaction system, rendering the differentiation of homopolymer numbers challenging. Different volumes of nucleotides were added to the reaction system, with the results shown in Figure S3. As illustrated in Figure 4(d), the experimental results indicated that homopolymer resolution was optimal when 0.8 µL of nucleotides was added; consequently, the final nucleotide addition volume was established at 0.8 µL.

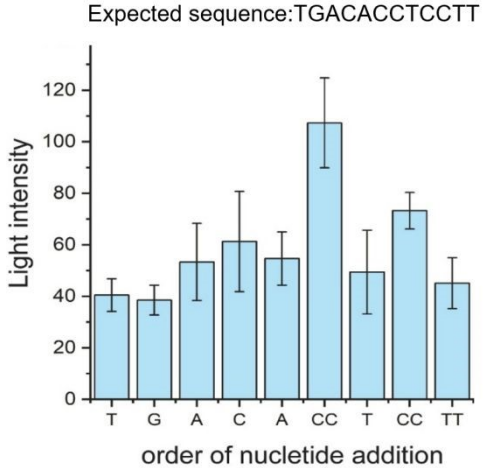

Fig.5 The sequencing results of the standard sequence.

3.3 Verification of experimental procedures

Following optimisation, the overall performance of the AM-DMF-based pyrosequencing system was validated using a synthetic standard influenza A sequence. The enzyme mixture, substrate mixture, and four nucleotides were injected into the chip. A pre-programmed pathway file was executed to achieve automated sequencing. Three parallel replicates were established for this experiment, and background noise signal interference was removed. The results, as shown in Figure 5, indicated that the measured sequences were consistent with the expected sequences. This fully validated the system's robust reproducibility and accuracy in gene sequence detection, as well as its superior resolution in distinguishing homopolymer number. The system exhibited high resolution in distinguishing homopolymer lengths, confirming its suitability for quantitative SNPs analysis.

3.4 *CYP2C19* genotype detection

The *CYP2C19* gene is a DNA sequence located on chromosome 10, belonging to the cytochrome P450 supergene family. It influences drug metabolism, with the most typical example being clopidogrel, an antiplatelet agent[27, 28]. This drug is primarily used to prevent and treat cardiovascular, cerebrovascular, and other arterial circulatory disorders caused by excessive platelet aggregation[29].

Due to significant inter-individual variability, differences in *CYP2C19* genotype can lead to pronounced variation in drug metabolic capacity, thereby significantly affecting therapeutic efficacy and clinical outcomes. As schematically shown in Figure 6(a), comprehensive genetic testing must be conducted prior to initiating drug therapy. As illustrated in Figure 6(b), under ideal conditions: GG (normal metabolizer) denotes both strands of the allele remain unmutated, with the single nucleotide site exhibiting a G peak height of 100%; GA (intermediate metabolizer) denotes one strand of the allele is mutated, with the single nucleotide site exhibiting G and A peak heights of 50% each; AA (poor metabolizer) denotes both strands of the allele being mutated, with the single nucleotide site exhibiting a 100% peak height for A. Based on the analysis of the test results, the corresponding genotype is accurately determined, thereby ultimately establishing the optimal drug dosage and implementing precise targeted treatment strategies.

To validate the system's feasibility, we randomly selected 12 samples containing GG, GA, and AA results from the completed testing pool. This was undertaken to comprehensively verify all possible genotype outcomes. As demonstrated in Figures 6(c) and (d), the results were consistent with those obtained using a commercial pyrosequencing instrument (PyroMark Q24), further substantiating the system's viability. The details are provided in Figure S4, S5 and Table S3. Notably, the proposed system reduced reagent consumption by approximately 50%, substantially lowering per-test cost. In addition, the compact footprint, operational flexibility, and scalability of the AM-DMF platform suggest potential advantages over conventional benchtop instruments, particularly for decentralised testing and resource-limited clinical settings. Given the limited sample size, the conclusions should be regarded as proof-of-concept.

View Article Online
DOI: 10.1039/D6SD00032K

ARTICLE

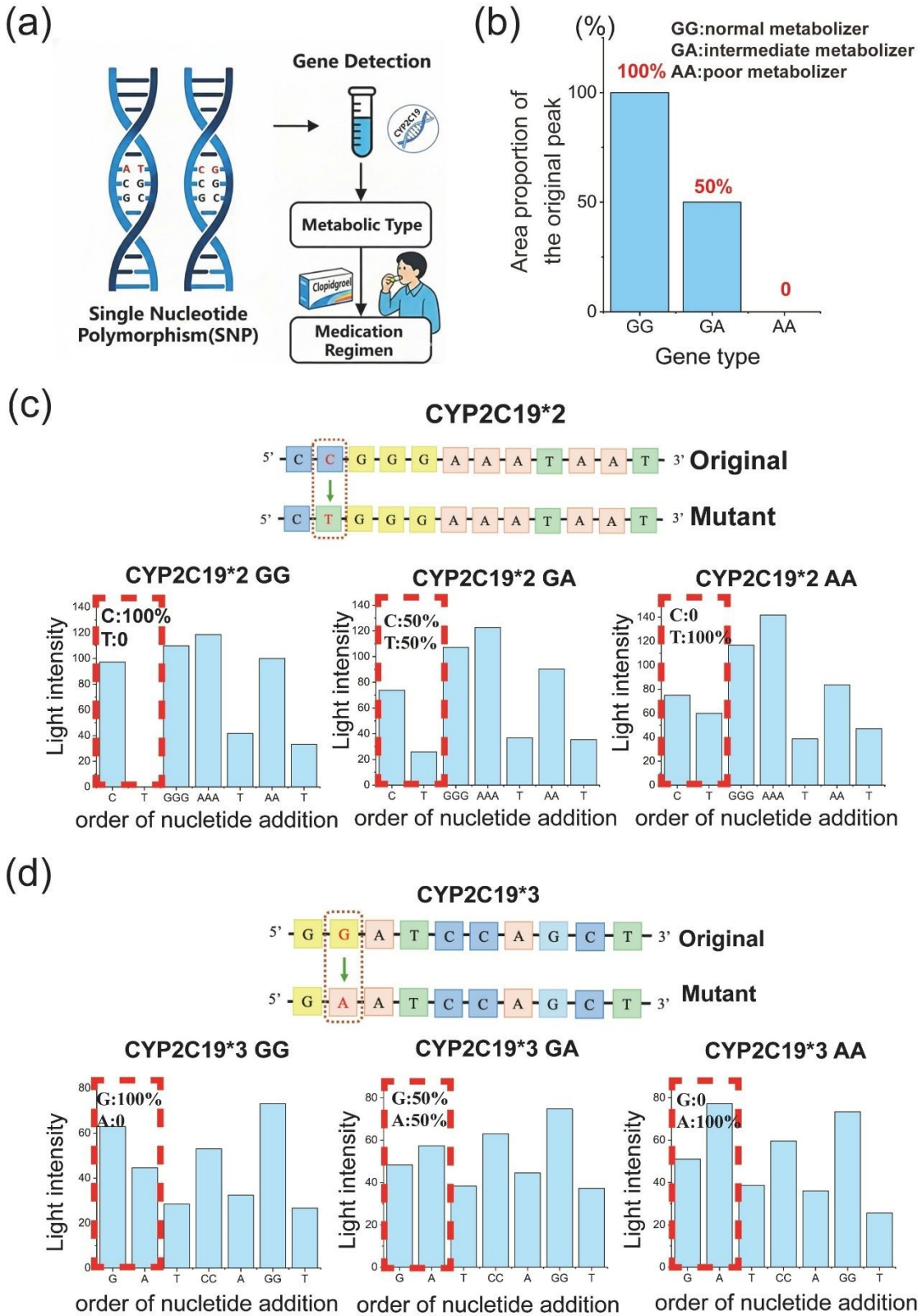

Fig.6 SNPs genotyping validation. (a) Drug Metabolism Detection Diagram. (b) Three metabolic phenotypes of the *CYP2C19* gene. (c) *CYP2C19*2* gene locus SNPs typing test results. (d) *CYP2C19*3* gene locus SNPs typing test results.

View Article Online
DOI: 10.1039/D6SD00032K

ARTICLE

4 Conclusions

In this work, we developed an AM-DMF-based pyrosequencing platform for rapid and automated SNPs detection, representing its first application in pharmacogenomic analysis. By integrating chemiluminescent signal detection with programmable droplet manipulation, the system enables fully automated reagent handling, reaction execution, and signal acquisition within a compact lab-on-a-chip format. Experimental validation demonstrated that single sample's SNPs analysis on-chip can be completed within 30 minutes. On-chip detection requires only 10 µL of sample, compared to the 20 µL used by commercial sequencers, thereby halving the reaction volume and reducing sequencing costs. Through *CYP2C19* gene testing of in 12 clinical samples confirmed 100% concordance with a commercial reference instrument, highlighting the system's accuracy and reliability. In this paper, we primarily focus on validating the on-chip pyrosequencing assay workflow; our team has already validated the feasibility of the pre-processing workflow[11, 12, 30]. It can therefore be demonstrated that the "sample-in, result-out" approach is feasible on the AM-DMF platform. The current AM-DMF technology route is scalable. High-throughput droplet movement and mixing operations (4,608 droplets, each with a volume of 0.9 nL) have already been successfully achieved[11]. An integrated circuit (IC) solution offers the potential for even higher throughput. Moving forward, we will design large-scale, high-density chips based on the number of samples and the test parameters to achieve this "sample-in, result-out" capability. Overall, the proposed platform represents a promising proof-of-concept for cost-effective, miniaturised, and automated pharmacogenomic testing, and may serve as a foundation for future clinical translation in precision medicine.

Author Contributions

H. H., T. W., Q. H., H. M. and S. H. conceived the design. H. H., T. W., Z. W., J. L. and S. H. designed the experiments. B. Z., T. W. ,H. H., K. J. and Z. C. performed experiments and wrote the manuscript. All authors reviewed and commented on the manuscript.

Conflicts of interest

There are no conflicts to declare.

Acknowledgements

This work was supported by National Key R&D Program of China (2023YFF0721500, 2024YFC3406900), Chinese Academy of Engineering Institute of Land Cooperation Consulting Project (Grant No. 2025-DFZD-39). The Science and Technology Innovation Project of Foshan, Guangdong Province, China (No.1920001000047), Guangdong Scientific and Technological Project (2025A0505010003), Jilin Scientific and Technical Development Program (20250204092YY), the Suzhou Basic Research Pilot Project (SSD2023013). We would like to thank Guangdong ACXEL Micro & Nano Tech Co. Ltd. for providing the chip-driven hardware and software system for this study.

Ethical Statement

All experiments involving human-derived samples were performed in accordance with the Declaration of Helsinki, relevant laws and institutional guidelines, and were approved by the Institutional Ethics Committee of the First Affiliated Hospital of Soochow University under the project entitled "CYP2C19 Genotyping Assay Kit (PCR-Fluorescence Probe Method)" (Ethics Approval/Registration No. 2021069). The human-derived samples used in this study were obtained from subjects enrolled in the Phase I Clinical Trial Unit of the First Affiliated Hospital of Soochow University. The requirement for informed consent was waived by the Institutional Ethics Committee.

Notes and references

Uncategorized References

1. G. Costain, R. D. Cohn, S. W. Scherer and C. R. Marshall, *Canadian Medical Association Journal*, 2021, **193**, E1626-E1629.
2. R. C. Novais and Y. R. Thorstenson, *Journal of Microbiological Methods*, 2011, **86**, 1-7.
3. A. Ahmadian, B. Gharizadeh, A. C. Gustafsson, F. Sterky, P. Nyrén, M. Uhlén and J. Lundeberg, *Analytical Biochemistry*, 2000, **280**, 103-110.
4. T. Nordström, M. Ronaghi, L. Forsberg, U. De Faire, R. Morgenstern and P. Nyrén, *Biotechnology and Applied Biochemistry*, 2010, **31**, 107-112.
5. A. Alderborn, A. Kristofferson and U. Hammerling, *Genome Research*, 2000, **10**, 1249-1258.
6. R. Sista, Z. Hua, P. Thwar, A. Sudarsan, V. Srinivasan, A. Eckhardt, M. Pollack and V. Pamula, *Lab on a Chip*, 2008, **8**.
7. M. Shen, Q. Wang, Q. Luo, J. Zhao and F. Shen, *Sensors & Diagnostics*, 2026, **5**, 26-41.
8. J.-C. Su, Y.-J. Liu and D.-J. Yao, *Micromachines*, 2022, **13**.
9. Z. Tong, C. Shen, Q. Li, H. Yin and H. Mao, *The Analyst*, 2023, **148**, 1399-1421.
10. S. Hu, J. Ye, S. Shi, C. Yang, K. Jin, C. Hu, D. Wang and H. Ma, *Analytical Chemistry*, 2023, **95**, 6905-6914.
11. J. Ji, X. Pang, C. Chang, D. Wang, S. Hu, Z. Fang, C. Yu, Q. Mei and H. Ma, *Angewandte Chemie (International ed. in English)*, 2025, **64**, e202501913.
12. Z. Yang, K. Jin, Y. Chen, Q. Liu, H. Chen, S. Hu, Y. Wang, Z. Pan, F. Feng, M. Shi, H. Xie, H. Ma and H. Zhou, *JACS Au*, 2024, **4**, 1811-1823.
13. H. Ma, S. Shi, K. Jin, D. Wang, S. Hu, Y. Su, Y. Zhang, J. Li, Z. Liu, C. Jiang, L. Feng, X. Guo and A. Nathan, 2020.

View Article Online
DOI: 10.1039/D6SD00032K

14. R. B. Fair, A. Khlystov, T. D. Tailor, V. Ivanov, R. D. Evans, V. Srinivasan, V. K. Pamula, M. G. Pollack, P. B. Griffin and J. Zhou, *IEEE Design & Test of Computers*, 2007, **24**, 10-24.
15. E. R. F. Welch, Y. Y. Lin, A. Madison and R. B. Fair, *Biotechnology Journal*, 2010, **6**, 165-176.
16. D. J. Boles, J. L. Benton, G. J. Siew, M. H. Levy, P. K. Thwar, M. A. Sandahl, J. L. Rouse, L. C. Perkins, A. P. Sudarsan, R. Jalili, V. K. Pamula, V. Srinivasan, R. B. Fair, P. B. Griffin, A. E. Eckhardt and M. G. Pollack, *Analytical Chemistry*, 2011, **83**, 8439-8447.
17. F. Zou, Q. Ruan, X. Lin, M. Zhang, Y. Song, L. Zhou, Z. Zhu, S. Lin, W. Wang and C. J. Yang, *Biosensors and Bioelectronics*, 2019, **126**, 551-557.
18. B. D. Sigurpalsdottir, O. A. Stefansson, G. Holley, D. Beyter, F. Zink, M. Þ. Hardarson, S. Þ. Sverrisson, N. Kristinsdottir, D. N. Magnusdottir, O. Þ. Magnusson, D. F. Gudbjartsson, B. V. Halldorsson and K. Stefansson, *Genome Biology*, 2024, **25**.
19. J. Xiao, C. Pu, X. Zhou, X. Zhang, S. Zhang, P. Yang, Y. Zhang and L. Xiong, *Frontiers in Medicine*, 2026, **12**, 1699607-1699607.
20. J. Shendure, G. J. Porreca, N. B. Reppas, X. Lin, J. P. McCutcheon, A. M. Rosenbaum, M. D. Wang, K. Zhang, R. D. Mitra and G. M. Church, *Science*, 2005, **309**, 1728-1732.
21. M. Ronaghi, *Genome Research*, 2001, **11**, 3-11.
22. F. Mugele and J.-C. Baret, *Journal of Physics: Condensed Matter*, 2005, **17**, R705-R774.
23. C. T. Harrington, E. I. Lin, M. T. Olson and J. R. Eshleman, *Archives of Pathology & Laboratory Medicine*, 2013, **137**, 1296-1303.
24. V. N. Luk, G. C. H. Mo and A. R. Wheeler, *Langmuir*, 2008, **24**, 6382-6389.
25. J. Li, N. S. Ha, T. L. Liu, R. M. van Dam and C.-J. 'Cj' Kim, *Nature*, 2019, **572**, 507-510.
26. S. H. Au, P. Kumar and A. R. Wheeler, *Langmuir*, 2011, **27**, 8586-8594.
27. L. Juan, X. Zesheng, L. Ya, D. Shipeng, L. Junying, P. Junjun and J. Yang, *Molecular membrane biology*, 2019, **35**, 1-8.
28. J. Schulte, L. Potzel, P. Frei, I. Seibert, K. Gerlach, K. M. C. Bender, E. Scheurer, H. E. M. Z. Schwabedissen and I. Schulz, *International journal of legal medicine*, 2026, DOI: 10.1007/s00414-025-03708-7, 1-13.
29. R. Mu, J. Gao, X. Wang, J. Ling, N. Hu and H. Yang, *Pharmaceutics*, 2025, **17**, 1582-1582.
30. C. Hu, C. Chang, M. Zhang, T. Peng, S. Hu, J. Li, J. Yu, C. Liao, M. Shi, A. Nathan, L. G. Occhipinti and H. Ma, *Small*, 2025, **21**.

View Article Online
DOI: 10.1039/D6SD00032K

Data availability

The data supporting this article, including representative raw photon-count traces/pyrograms, processed SNP-calling results, and additional experimental details, are provided in the Electronic Supplementary Information (ESI). De-identified patient-related genotyping data are available from the corresponding author upon reasonable request, subject to ethical and/or confidentiality restrictions and completion of an appropriate data sharing agreement where required.